Journal of Applied Sciences and Nanotechnology

Journal homepage: jasn.uotechnology.edu.iq

Analysis Study of Antibacterial Efficacy and Cytotoxicity of Prepared Metal-Based Nanoparticles against *Streptococcus mutans*: Focus on Gold Nanoparticles

[1]Fattin A. Fadhil*, [2]Azhar M. Haleem, [1]Abdulrahman Khalaf Ali, [3]Ahlam T. Mohammed

[1]Department of Applied Sciences, University of Technology - Iraq, Iraq
[2]Environmental Research Center, University of Technology - Iraq, Iraq
[3]College of Dentistry, University of Baghdad, Iraq

A R T I C L E I N F O

Article history:
Received: January, 06, 2025
Accepted: April, 02, 2025
Available online: June, 10, 2025

Keywords:
Gold Nanoparticles,
UV-VIS,
TEM,
Streptococcus mutants

****Corresponding Author:***
Fattin A. Fadhil
fattin.a.fadhil@uotechnology.edu.iq

A B S T R A C T

New approaches have been developed to combat bacterial infections because of the growing threat of antibiotic-resistant bacteria. Gold colloidal nanoparticles and their applications as antibacterial agents have shown promising strategies due to these properties. The properties of nanoparticles, including size, shape, and surface charge, play an essential role in determining antibacterial activity. Pulsed laser ablation in a liquid medium was utilized to produce gold nanoparticles, an environmentally friendly method. Gold NPs were produced in ultrapure water. Experimental research was done to determine the impact of the number of laser pulses on the nanoparticles' size, shape, and concentration. Surface plasmon resonance (SPR) peaks for gold nanoparticles were detected by UV–visible spectroscopy at approximately 525 nm in the visible region. Transmission electron microscopy (TEM) showed the appearance of spherical nanoparticles with an average size of 20 to 80 nm. For gold nanoparticles, increasing laser pulses from 100 to 250 pulses while maintaining the fixed energy of the laser at 600 mJ reduced the average nanoparticle size. *S. mutans* were isolated to study and evaluate the antibacterial effects of AuNP substances using the suitable diffusion method. The antibacterial examination revealed valuable results for gold nanoparticles, which showed a more significant effect on bacteria at high concentrations. The best results were found for the sample prepared at the highest concentration at 250 pulses. Toxicity assessments of the materials revealed low toxicity levels of this material, confirming their safety for human use.

https://doi.org/10.53293/jasn.2025.7566.1333, Department of Applied Sciences, University of Technology - Iraq.

1. Introduction

Dental caries is a major worldwide health issue affecting people of all ages [1]. Demineralization of tooth enamel and dentin is a significant cause of tooth decay caused by acidic by-products produced during the metabolic processes of oral bacteria, especially *Streptococcus mutans* (*S. mutans*) [2]. These bacteria have been identified as a major contributor to dental caries due to their ability to form biofilms on tooth surfaces and produce acids in a carbohydrate-rich environment [3]. Despite advancing prevention methods, dental caries remain a significant health challenge worldwide [4]. Conventional methods of treating caries cases have been adopted based on mechanical removal of decayed tissue followed by restorative procedures or the use of fluoride to promote remineralization [5]. Although these methods have proven effective, they do not directly treat bacterial infections or offer lasting protection against recurrent caries [6]. Nanotechnology has emerged as a potential subject in dental care advancement, introducing revolutionary approaches for diagnostics and treatment. Among several materials that have gained popularity, nanogold is particularly appealing due to its unique physical and chemical characteristics and antibacterial potential [7]. Recent studies have shown that nanogold has a great potential to disrupt biofilms and exhibit bactericidal effects against *S. mutans*, which makes it a promising candidate for combating dental caries at its microbial origin [8]. In the current study, the results will be adopted in an application that consists of strengthening and enhancing the resistance of teeth to caries while targeting *S. mutans* at the same time. Based on previous research, we explored the incorporation of nanogold particles into dental caries structures. We evaluated its effect on remineralization of tooth enamel and disruption of biofilms, unlike previous studies focusing only on antimicrobial effects.

Laser ablation in liquid (LAL) has become a valuable and flexible way to create nanomaterials with unique characteristics [9, 10]. This innovative technology in a liquid environment uses laser pulses to induce physical and chemical processes that produce nanoparticles and nanostructures with precise size, shape, content, and structure. The ability of LAL to modulate critical parameters at the nanoscale makes it a potentially important tool in a range of scientific fields, including materials science, chemistry, biology, and medicine [11]. Laser ablation in liquids (LAL) is when a high-intensity laser beam is directed at a target material submerged in a liquid medium. Upon interaction with the laser, the target material rapidly vaporizes and forms a plasma plume. The adjacent liquid environment controls heat transfer dynamics and plasma-derived nanocrystal nucleation and growth. This method allows the production of various types of nanoparticles from metals, including metallic gold and platinum, metal oxides, and other more complex nanoscale architectures [12]. A key advantage of LAL is the ability to generate nanoparticles without requiring stabilizing agents or surfactants, minimizing contamination and simplifying their use in applications such as environmental remediation, biomedicine, and catalysis. Furthermore, the controlled synthesis of LAL makes it possible to precisely modify nanoparticles' optical and catalytic properties for specific applications [13, 14].

2. Experimental Part

This experimental study was conducted in a laboratory setting, where antibacterial tests were performed at the Microbiology Laboratory of the Environmental Research Center, University of Technology in Baghdad, Iraq, and nanoparticles were synthesized in the laser laboratory of the College of Applied Sciences.

2.1 Materials and Sample Preparation

High-purity gold plates (99.9%) were procured from Danyang Xinli Alloy Company (China), and their composition was verified using X-ray diffraction (DX 2700 AB) with a Cu-Kα target. The plates were then cut into 1 × 2 cm pieces, polished with abrasive paper, and thoroughly cleaned with ethanol and deionized water (DIW) before synthesis.

2.2 Synthesis of Gold NPs

A suitable liquid medium or solvent was selected based on the required properties of the nanoparticles. In this study, DIW was used. A gold plate was placed at the base of a cylindrical glass vase containing 2 milliliters of DIW. Using different laser pulses (100, 150, 200, and 250) at room temperature and ambient pressure, a Q-switched pulsed Nd: YAG laser with a 1064 nm wavelength, 600 mJ of laser energy, and a 1 Hz repetition rate was used to treat the object that was immersed. The optimal distance between the lens and the bottom of the target was set at 8 cm, as this provided the softest sound, indicating minimal disturbance while achieving the smallest particle ablation from the target. When the laser pulse hits the surface of the target material, it causes energy absorption and rapid heating, thus melting the target material. When the laser energy density is high enough, the surface of the target is subjected to evaporation or sublimation, leading to the formation of a plasma column. The plasma column that arises from the interaction between the high-energy laser pulse and the solute consists of ions, electrons and evaporated materials. This column expands at a tremendous speed in the liquid environment due to the high temperature and pressure [15]. A shock wave is generated in the liquid due to this expansion, which will cause local heating and the generation of cavity bubbles. The bubble grows as the evaporated material and gases escape from the plasma. The bubble will then collapse due to the pressure of the liquid after reaching the critical size due to the expansion, where the collapse leads to the generation of harsh conditions (high pressure and temperature), causing the solute to decompose into smaller particles. The solute condenses in the cooled liquid, forming nanoparticles. The nanoparticles' size, shape, and composition are determined by the laser parameters (wavelength, pulse duration, and flux), the target material, and the quality of the liquid medium [16]. The schematic design of the experimental apparatus is shown in **Fig. 1.**

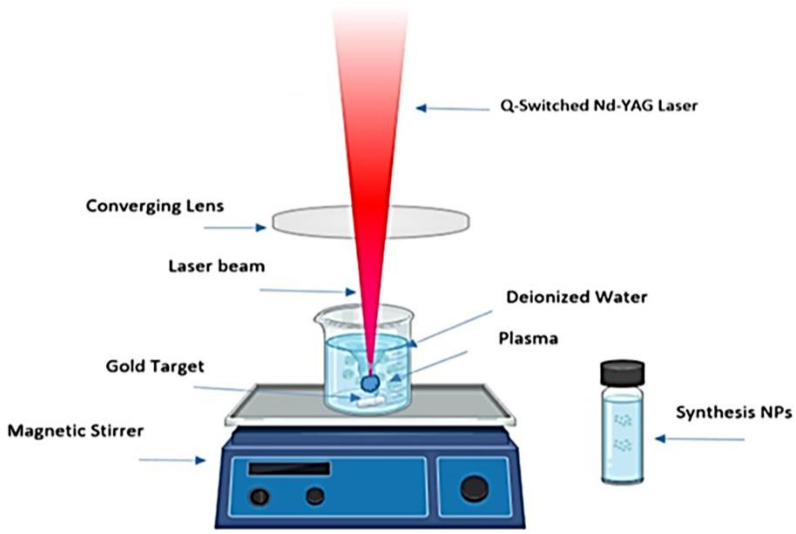

Figure 1: laser setup for nanoparticle preparation.

2.3 Zeta Potential (ZP)

A Malvern Panalytical Zeta Potential Analyzer was employed to evaluate nanoparticle stability. The device measured the zeta potential of colloidal particles using laser Doppler electrophoresis, which detects the Doppler shift in scattered light resulting from particle motion.

2.4 Antimicrobial Activity Assay

The *S. mutans* bacterial isolate was obtained from the Environmental Research Center at the University of Technology in Baghdad, Iraq, and used to evaluate the impact of the synthesized nanomaterials on bacterial viability under ex vivo conditions. This isolate was cultured on a Nutrient Agar medium. The effects of nano-elements generated at concentrations of (0.0, 5, 10, 15, 20, 25) µg/mL for each element (Au) were investigated using the Well Diffusion Method using the following stages.

1. To activate the bacteria, they were cultured in brain infusion broth and incubated in a shaking incubator at 200 rpm for 24 hours at 37 °C.
2. To examine the antibacterial effect, the activated bacteria were separated on Muller Hinton media surface. Next, the medium was prepared with equal-diameter, each 6 mm diameter to accommodate the nano-element solution with different concentrations, and the plates incubated for 24 hrs. at 37 °C.
3. The inhibition zone diameter around the holes can be measured using a ruler, and then calculate the inhibiting rate using the **Eq. (1)** [17]:

$$Inhibition\,percentage\ =\ test\ reading\ /\ control\ reading\ x100\% \tag{1}$$

2.5 Cytotoxic Assay of AuNPs Prepared at Different Laser Pulses

A healthy 25-year-old male had a vinous puncture to collect 10 mm of whole blood. Following that, blood was extracted with a sterile syringe coated with anticoagulant, poured into a sterile test tube with screw cover, and centrifuged for five minutes at 5000 rpm/min. To investigate the toxic effect of the prepared nanoparticles on these cells, the top layer of white blood cells, also known as buffy white blood cells, was harvested using a sterile glass Pasteur pipette and added to a test tube containing 5 ml of sterile RPMI-1640 medium supplemented with 10% fetal calf serum (FCS).

This resulted in a white blood cell concentration of 1×104/mL. To investigate the toxic effect on white blood cells, increasing doses of AuNPs (0, 25, 50, 100 and 200 µg/mL) were inserted into the culture of free serum (RPMI -1640). The experimentation was achieved using a 96-well microliter plate of flat-bottom. Each sample well was inoculated with 100 µL WBC suspensions hold 1×10^4 cell per mL and submitted to the pre-doses. The plates were placed in the incubator at 37 °C for 24 hours. Column #1 used and denoted negative control. After the incubation, all plates were slosh and then washed in PBS four times. finally, 10 µL at concentration of 0.5 mg/mL of (MTT) dye were added to all samples. All cells were washed many times using PBS until the dye was clear. The results were recorded by ELISA spectrophotometer at 500 nm.

2.6 Ablated Amount of NPs

Apply a 5-digit sensitive balance to weigh the empty tube (M empty) and then add 5 mL of the final product to get the concentration of colloidal NPs in micrograms per milliliter. Using an oven will help remove the water from the colloidal NPs in the tube. Weigh the dry tube (M dried) at the conclusion. This easy formula was used to calculate the concentration (C) of NPs, and it is empirical equation **Eq. (2).**

$$C = \frac{\text{M dried} - \text{M empty}}{\text{Liquid Volume}}\ (\mu\text{g/mL}) \tag{2}$$

2.7 Statistical Analysis

Data were analyzed using two-way analysis of variance (ANOVA) and given as mean ± SD for three repeats of every test using SPSS software version 22. The Least Significant Difference (LSD) was calculated at $p < 0.05$.

3. Results and Discussions

3.1 The Mass Concentration of AuNPs

Fig. 2 demonstrates the impact of laser pulses on the amount of gold (Au) nanoparticles ablated when the bulk target was laser-ablated in deionized water. The ablated quantities for gold nanoparticles were (87, 132, 192, and 245) µg/mL as in **Eq. (2).**

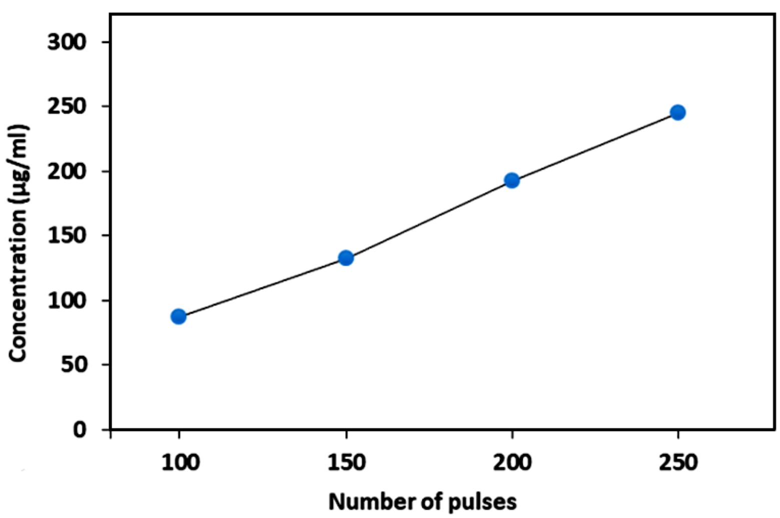

Figure 2: The mass concentration of AuNPs created by laser ablation in water varies with the number of laser pulses.

3.2 UV-vis Absorption Investigation

The ablated quantities for gold nanoparticles were (87, 132, 192, and 245), µg/ml. (Equations 2). This study presents the optical characterization of gold nanoparticles prepared at 600 mJ under various pulse values (100, 150, 200 and 250) as shown in Figure 3. The optical properties were evaluated at a characteristic wavelength of 1064 nm, revealing significant trends in absorbance behavior with varying laser pulses. Results show an advantageous correlation between the number of laser pulses and the absorbance of the produced Au NPs. This trend suggests an enhancement in particle concentration or structural evolution of the material had been ablated as the laser's interaction with the medium progressed [18]. The structure, shape, metal, and size of AuNPs affect the band intensity and wavelength [19, 20]. For spherical AuNPs of 10 nm, the surface plasmon band usually exhibits peaks in the UV-Vis range of 520 nm. As the diameter of NPs increases, the wavelength changes to larger values [21]. The synthesized AuNPs exhibited a distinct broad peak at 520 nm. Based on this observation, the AuNPs had an estimated diameter of around 10 nm. The increase in absorbance with pulse count could be attributed to several interrelated factors, such as increased material ablation, where with higher pulse counts, the cumulative ablation of the target material likely generates a higher concentration of nanoparticles or colloidal species in the liquid medium. This increase would enhance light-matter interaction, leading to higher absorbance. The second reason is particle growth and aggregation, where prolonged laser exposure may facilitate the development or aggregation of nanoparticles due to localized heating and pressure effects. Such particle size and morphology changes often influence optical properties, including absorbance. As the particle density increases, scattering effects might also contribute to the increased absorbance, especially at a wavelength of 1064 nm. At this wavelength, scattering from nanostructures becomes more significant, contributing to the observed rise in absorbance [22]. The wavelength-specific absorbance at 1064 nm may also hint at resonance phenomena or specific vibrational or electronic transitions within the synthesized material. We notice an increase in the absorption peak of the gold nanoparticle with the rise in the number of laser pulses, as shown in **Table 1**. The peak position in the absorption spectra of AuNPs was at the visible area (about 525 nm) due to SPR, which is consistent with previous [23].

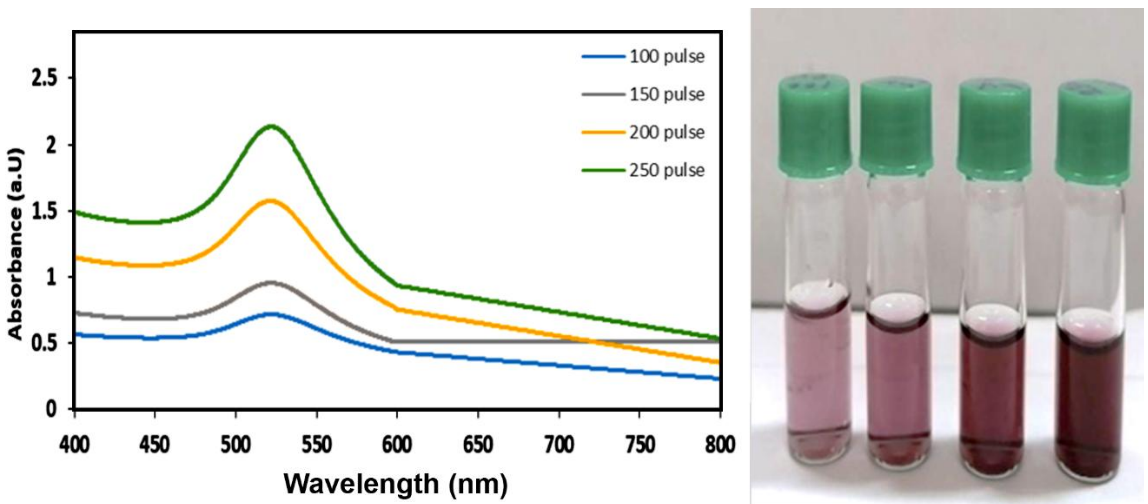

Figure 3: (a) Ultraviolet-visible absorption spectrum of AuNPs that are prepared by pulsed laser ablation in liquid, for different pulses (100,150,200,250) and (b) Au NPs colloidal

Table 1: Surface plasmon resonance (SPR) of colloidal gold nanoparticles

Nanoparticle Types	Number of pulses	Absorbance (arb. units)
Au NPs	**100**	**0.716**
	150	**0.953**
	200	**2.416**
	250	**2.611**

Fig. 4 shows the Zeta potential distribution of AuNPs (at 250 pulses). This test helps understand and improve the dispersion of nanoparticles in different media as the surface charge affects cellular uptake and interaction with biological membranes. For gold nanoparticles, the zeta potential usually appears in the range of -20 mV to -40 mV. Because of the chemistry on their surface, gold nanoparticles frequently have a high zeta potential. Depending on their production process and stabilizers, gold particles usually exhibit a zeta potential when suspended in deionized water [24].

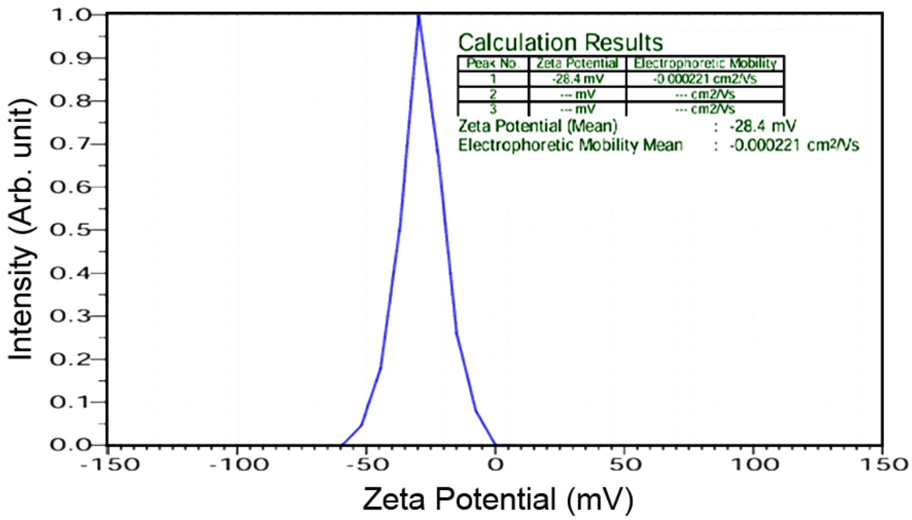

Figure 4: Zeta potential distribution curves were used in stability tests of AuNPs (at 250 pulses).

3.4 Structure Properties

Fig. 5 shows the X-ray diffraction of the gold plate in water at 250 pulses. XRD measurements were examined by Cu Kα source (1.5406 A). The measured samples were prepared by using the drop-casting technique. The samples were dried using an electric oven to reach the required thickness. The diffraction peaks at 38.184°, 44.277°, 64.426° and 77.472° indicate reflection from the (111), (200), (220), and (311) crystal planes in the cubic structure of Au NPs according to Card No. 04-0784. The grain size was estimated using the Scherrer equation **Eq. (3)** in agreement with SEM results. **Table 2** provides XRD data for experimental Au NPs, including peak position, crystalline size variation, FWHM, and miller index (hkl) [25].

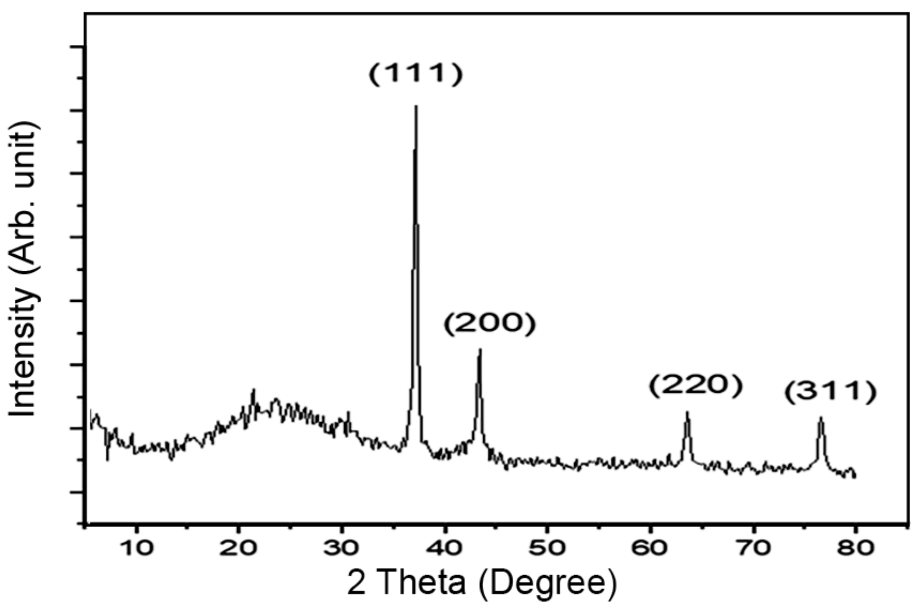

Figure 5: X-ray diffraction of the gold plate.

Table 2: The 2-Theta, FWHM, Miller indices, and crystalline size of AuNPs.

2θ (deg.)	FWHM (deg.)	d_{hkl} (Å)	$a_{\circ}$ (Å)	Miller indices (hkl)	Crystallite Size (nm)	Crystall System	Card Number
38.184°	0.498	2.3	3.98	111	18	Cubic	04-0784
44.277°	0.657	2.0	4.00	200	14	Cubic	04-0784
64.426°	0.993	1.4	3.95	220	10	Cubic	04-0784
77.472°	1.064	1.2	3.97	311	10	Cubic	04-0784

$$\boldsymbol{D} = 0.89\lambda/\beta \cos\theta \tag{3}$$

Where D is the grain size, λ is the wavelength of light used for diffraction, β is the "full width at half maximum" of sharp peaks, and θ is the observed angle. From the equation below, the lattice constant (a) was also calculated [26]:

$$\boldsymbol{d} = \frac{\boldsymbol{a}}{\sqrt{\boldsymbol{h}^2+\boldsymbol{k}^2+\boldsymbol{l}^2}} \tag{4}$$

Where the d-spacing can be estimated from the following **Eq. (5)** [25]:

$$\boldsymbol{d} = \frac{\lambda}{2sin\theta} \tag{5}$$

3.5 Morphologies of AuNPs

Fig. 6 displays field emission scanning electron microscope (FESEM) images of AuNPs produced with different laser shots, specifically 100, 150, 200, and 250 pulses, 600 mJ laser energy, and 1064 nm wavelength. The production of nanoparticles using PLAL resulted in a notable decrease in the particle size of gold nanoparticles with increased laser pulses. SEM (scanning electron microscopy) analysis revealed that as the density of the substance increased during the ablation process, the resulting nanoparticles exhibited a reduced average size. This trend suggests that higher concentration promotes more effective nucleation and growth processes, leading to finer particles.

The reduced particle size is crucial for enhancing the surface-to-volume ratio, which is beneficial for applications in catalysis, drug delivery, and other nanotechnology fields. These results are consistent with earlier research., underscoring the potential of PLAL as a versatile and effective method for tailoring nanoparticle properties by adjusting experimental parameters [27].

TEM images of colloidal AuNPs created using a Nd: YAG laser with a wavelength of 1064 nm, an energy of (600) mJ, and a range of laser pulses (100 to 250) are shown in **Fig. 7**.

In the research, the TEM examination showed a significant pattern in the dimensions of the nanomaterial created from a substance gold target with high purity through the PLAL method. As the concentration of AuNPs rose, the dimensions of the produced nanomaterials steadily diminished, demonstrating an inverse correlation between precursor concentration and nanoparticle dimensions. This occurrence can be linked to the increased collision rate and energy exchange during the laser ablation process, resulting in more effective fragmentation of the nanomaterials [28]. With an increasing number of laser pulses, the fragmentation of the formed nanoparticles also increased. However, particle aggregation was occasionally observed at higher concentrations. This aggregation facilitated particle growth through recrystallisation or agglomeration.

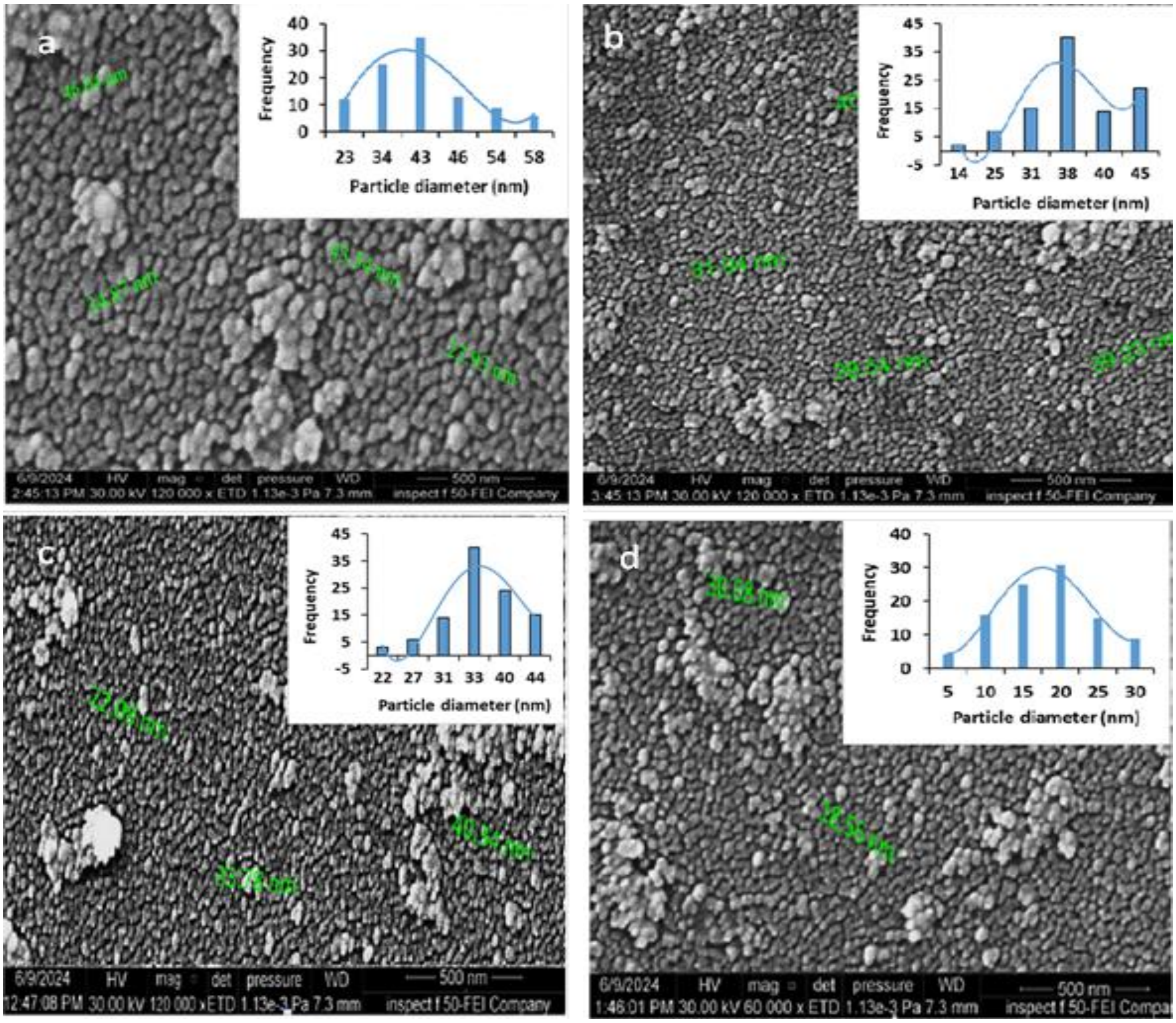

Figure 6: FESEM images of AuNPs generated with varying laser pulse numbers ((a)100 pulses, (b) 150 pulses, (c) 200 pulses, (d) 250 pulses)

Additionally, a higher pulse count sometimes led to an inhomogeneous particle distribution, resulting in a mixture of small and large nanoparticles due to continuous interaction with subsequent pulses. Nevertheless, the prevailing majority are tiny particles. These results align with earlier studies that show comparable size reduction effects as precursor concentration increases in PLAL processes [29]. Some nanoparticles were smaller than 10 nm and between 50 and 60 nm. The nanoparticles predominately exhibited a spherical shape. However, other morphologies of Au NPs were also observed. The smaller size boosts the surface-to-volume ratio, which is advantageous for catalytic and optical uses while improving the nanomaterials' stability and disposability. This behavior is essential for improving the performance of nanomaterials in diverse applications, making this research a valuable contributor to the field.

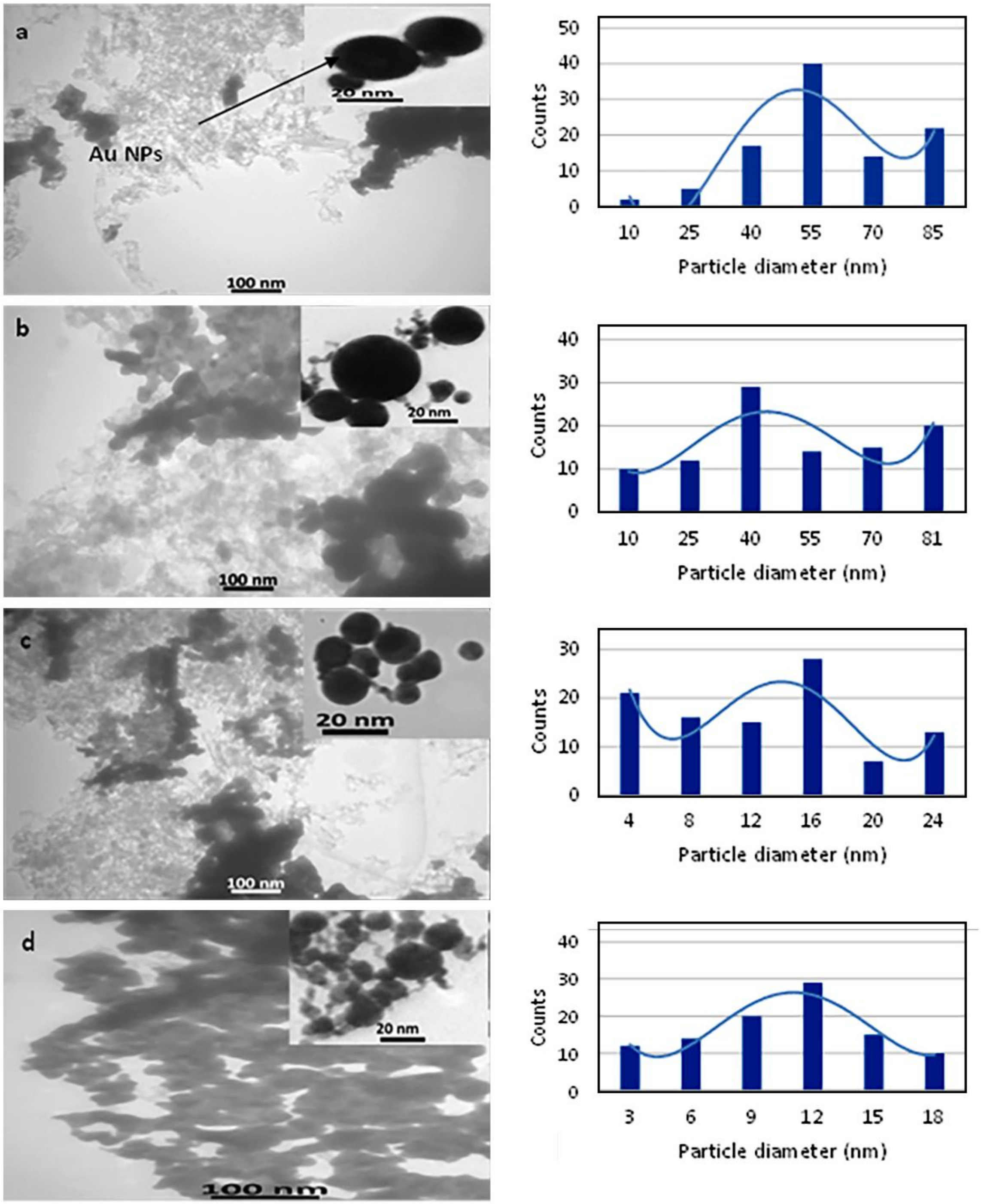

Figure 7: TEM images (left) and size distribution (right) of AuNPs produced using 600 mJ of energy and various laser pulses ((a)100 pulses, (b)150 pulses, (c) 200 pulses, and (d) 250 pulses).

3.6 The Activity of Antibacterial for AuNPs

Gold antibacterial was examined against *S. mutant*. The inhibition zone of pre-treated AuNPs is illustrated in **Table 3** and **Fig. 8**. The AuNPs at doses of 0.0,5, 10, 15, 20 and 200 μg/mL showed enhanced antibacterial. The positive control was 0.2% chlorhexidine with an inhibition zone of 25 mm. *S. mutans* highly virulent bacteria possess a set of virulence factors that enable them to invade the tooth and change its external shape by secreting a set of enzymes such as Proteases, phospholipase, Glucosyltransferases (GTFs), Lactate dehydrogenase (LDH) and other enzymes that work to erode the tooth's basic material. These bacteria work together with other species to invade the teeth, causing permanent and severe damage. Their mechanism of action depends on the acidic function of the mouth and local immunity, so we see that children, pregnant women, and those with chronic diseases are more susceptible to tooth decay due to weak local immunity. Gold nanoparticles were tested to determine their activity against *S. mutans* to evaluate the effectiveness of different concentrations of antibacterial nanoparticles. As shown in **Table 3**, there were significant differences at the probability level (P ≤0.05) between the number of different pulses during preparation, and the highest level of inhibition was at the pulses number of 250 pulses [30].

Table 3: The inhibitory effects of AuNPs on *S. mutans* using a diffusion method at different concentrations and laser pulses.

Conce. (μg/mL)	M±SD 100 pulses	IR1%	M±SD 150 pulses	IR2%	M±SD 200 pulses	IR3%	M±SD 250 pulses	IR4%
0.0	0.0	0.0	0.0	0.0	0.0	0.0	0.0	0.0
5	7.2±0.125*	47.18	7.4±0.07 *	48.49	7.3±0.22 *	47.83	7.5±0.19 *	49.14
10	8.8±0.15 *	57.66	8.6±0.17 *	56.35	8.7±0.14 *	57.01	8.6±0.25 *	56.35
15	9.6±0.13 *	62.90	9.9±0.15 *	64.87	9.3±0.18 *	60.94	9.4±0.33 *	61.15
20	10.2±0.12 *	66.4	10.1±0.12 *	66.18	10.1±0.16 *	66.18	10.12±0.21 *	66.31
25	11.7±0.14 *	76.67	11.3±0.22 *	74.04	11.5±0.15 *	75.36	11.4±0.17 *	74.70
0.2 % Chlorhexidine	15.26±0.20				P-value = 0.998			

number show M±SD at 3 replicates * P≤0.05

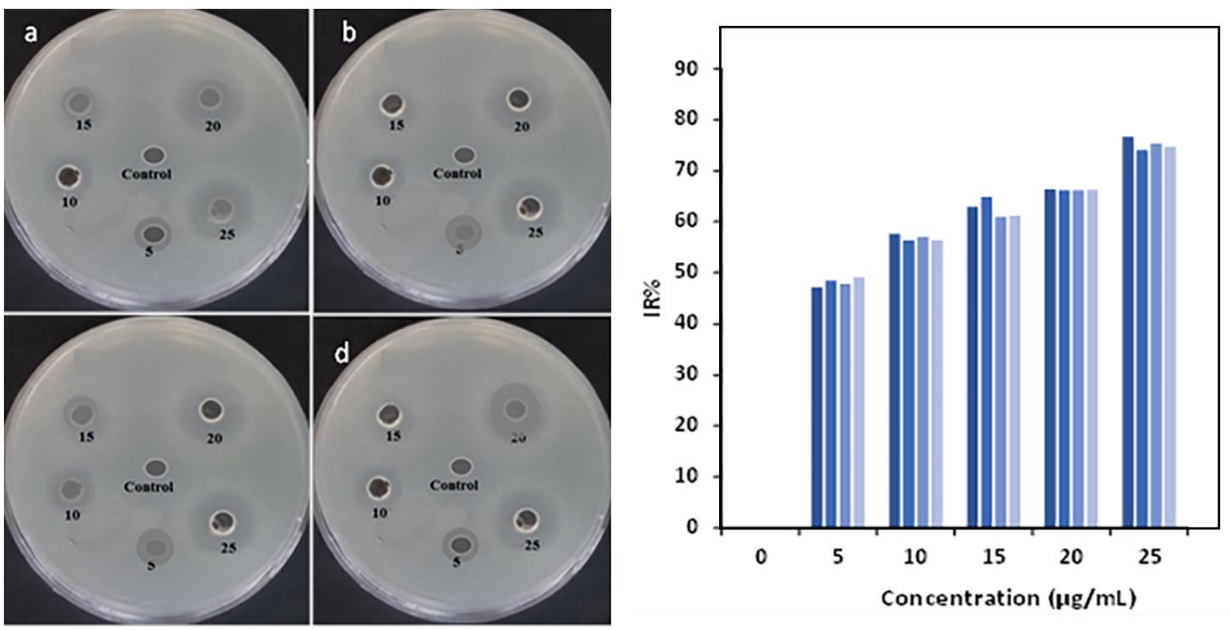

Figure 8: The inhibitory effects of AuNPs on *S. mutans* using well diffusion method at different laser pulses ((a) 100 pulses, (b) 150 pulses, (c) 200 pulses, (d) 250 pulses) (left). The Inhibition rate of *S. mutans* treated AuNPs (right).

The inhibition was strongly associated with concentration, as the inhibition zone expanded with increasing concentration until the inhibition rates reached 76% at a concentration (25 μg/mL**)**; however, it did not overcome the positive control. Oxidative stress, heterogeneous embryonic changes, protein disruption, and electrolyte imbalance are caused by the interaction between the prepared nanoparticles and nucleic acid, lysosomes, ribosomes, and enzymes of the bacteria. In addition, nanoparticles can change gene expression and inhibit proteins, the leading cause of cell death [31].

3.7 Cytotoxic Assay

Mossman's Tetrazolium Toxicity Assay (MTT) is the most widely used method for determining the cytotoxic effects of various chemicals under different concentrations or conditions; as shown in **Table 4**, **Fig. 9**, toxicity measurement is an important measurement that represents a fascinating trend. We observed an apparent decrease in the toxicity of the materials as a function of increasing nanomaterial concentrations. This finding differs from general expectations, as toxic risks are usually associated with increasing concentrations of nanomaterials. At low concentrations, nanomaterials maintain their large surface area and reactivity, which leads to increased production of reactive oxygen species (ROS). These levels are an established pathway for nontoxicity and thus will cause oxidative stress, cell damage, and inflammation [32]. At high concentrations, this may lead to the aggregation of nanomaterials into larger aggregates, reducing the reactive surface area and their interactions with cellular components. Thus, toxicity another factor that may be very influential is that high nanomaterial concentrations may lead to cellular saturation and thus limit absorption, which causes a decrease in the concentrations of these particles inside the cells [33]. Therefore, this decrease in toxicity can be explained by a reduction in cellular exposure. The results obtained align with previous literature, as evidenced by a study conducted by [34] that showed low toxicity at high concentrations of nanomaterials, which explains the accumulation of these particles and the decrease in biocompatibility. Understanding the interaction between concentrations and biological effects emphasizes the significance of these results, as the low toxicity of nanomaterials, despite their small size, is promising for biomedical and environmental safety. Typically, smaller nanoparticles exhibited higher toxicity, but in this case, their low toxicity may be attributed to the agglomeration that occurs when concentrations increase, thus reducing biocompatibility [35][36].

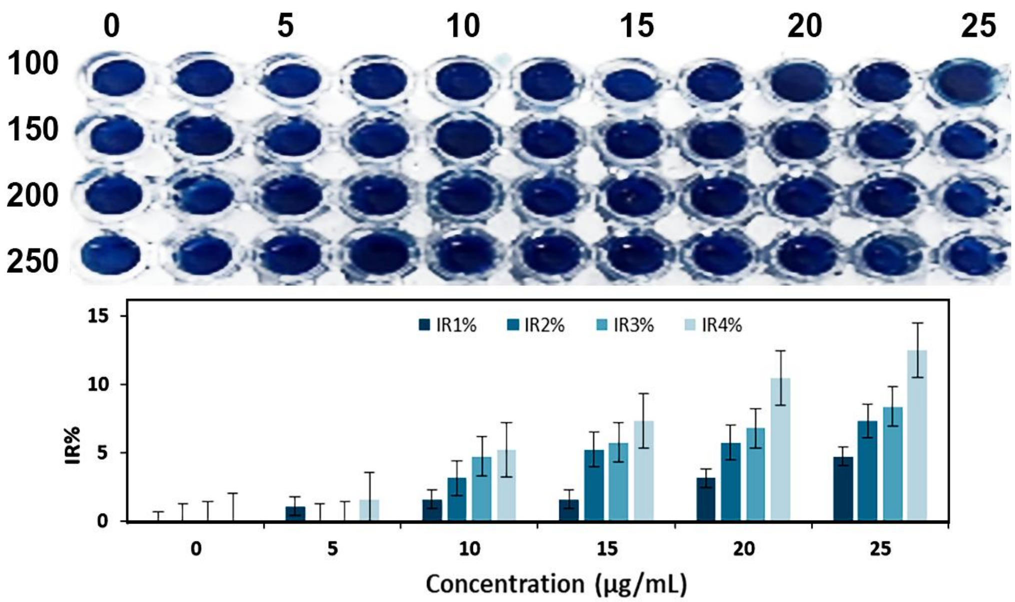

Figure 9: The cytotoxicity by MTT assay on healthy white blood cells (WBCs) at different concentrations of AuNPs that have prepared on different pulses (up), Inhibition rate (%) of white blood cells treated with AuNPs (down).

Table 4: Summarize of the MTT assay for AuNPs at various concentrations on WBC.

Conce. (µg/mL)	Absorbency 100 pulses	IR1%	Absorbency 150 pulses	IR2%	Absorbency 200 pulses	IR3%	Absorbency 250 pulses	IR4%
0.0	1.91	0.0	1.91	0.0	1.91	0.0	1.91	0.0
5	1.89	1.04	1.91	0.0	1.90	0.0	1.88	1.57
10	1.88	1.57	1.85	3.14	1.82	4.71	1.81	5.23
15	1.88	1.57	1.81	5.23	1.80	5.75	1.77	7.32
20	1.85	3.14	1.80	5.75	1.78	6.80	1.71	10.47
25	1.82	4.71	1.77	7.32	1.75	8.37	1.67	12.56

4. Conclusion

The most important finding of this work is that PLAL is fast, cost-effective and environmentally friendly. SEM, TEM and UV-VIS helped to reveal the production process of the nanoparticles as well as their size, shape and other properties. When studying surface morphology, it was found that the size of the nanoparticles decreased as the number of laser pulses increased. This can be attributed to the fact that the ablated particles can absorb more laser energy and thus break down into smaller particles. The study shows that the antibacterial activity increases as the size of the gold nanoparticles decreases. This size-dependent effect is due to the improved surface-to-volume ratio, which promotes better contact with the bacterial cells. The results show the importance of optimizing particle size in the production of nanomaterials for antibacterial applications. These results support previous research and show the possibility of gold nanoparticles as effective antibacterial agents. However, the ability of nanoparticles to influence cell structure has been greatly improved.

Conflict of Interest

The authors declare that they have no conflict of interest.

References

[1] R. A. Bagramian, F. Garcia-Godoy, and A. R. Volpe, “The global increase in dental caries. A pending public health crisis,” *Am J dent*, vol. 22, no. 1, pp. 3–8, 2009.

[2] S. E. Cross, J. Kreth, R. P. Wali, R. Sullivan, W. Shi, and J. K. Gimzewski, “Evaluation of bacteria-induced enamel demineralization using optical profilometry,” *Dent. Mater.*, vol. 25, no. 12, pp. 1517–1526, 2009.

[3] A. F. P. Leme, H. Koo, C. M. Bellato, G. Bedi, and J. A. Cury, “The role of sucrose in cariogenic dental biofilm formation—new insight,” *J. Dent. Res.*, vol. 85, no. 10, pp. 878–887, 2006.

[4] P. Y. F. Wen, M. X. Chen, Y. J. Zhong, Q. Q. Dong, and H. M. Wong, “Global burden and inequality of dental caries, 1990 to 2019,” *J. Dent. Res.*, vol. 101, no. 4, pp. 392–399, 2022.

[5] A. Warreth, “Dental caries and its management,” *Int. J. Dent.*, vol. 2023, no. 1, p. 9365845, 2023.

[6] M. J. Y. Yon, S. S. Gao, K. J. Chen, D. Duangthip, E. C. M. Lo, and C. H. Chu, “Medical model in caries management,” *Dent. J.*, vol. 7, no. 2, p. 37, 2019.

[7] S. Malik and Y. Waheed, “Emerging applications of nanotechnology in dentistry,” *Dent. J.*, vol. 11, no. 11, p. 266, 2023.

[8] K. Selvaraj, L. S. Venkatesan, D. Ganapathy, and P. Sathishkumar, “Treatment of dental biofilm-forming bacterium Streptococcus mutans using tannic acid-mediated gold nanoparticles,” *Microb. Pathog.*, vol. 189, p. 106568, 2024.

[9] F. A. Fadhil, “Gold Nanoparticles Synthesized by Laser Ablation in Water: Optical and Structural Characterizations,” *Eng. Technol. J.*, vol. 33, no. 8 Part (B) Scientific, 2015.

[10] B. A. Bader, I. H. Hadi, M. Y. Slewa, K. S. Khashan, and F. A. Abdulameer, “Photodetector Based on Titanium Oxide Nanoparticles Produced via Pulsed Laser Ablation,” *Adv. Condens. Matter Phys.*, vol. 2022, no. 1, p. 8066167, 2022.

[11] O. A. Lazar, A. S. Nikolov, C. C. Moise, and M. Enachescu, “Pulsed Laser Ablation in Liquids for Fabrication of Noble Metal Nanostructures,” in *Laser Ablation-Applications and Modeling*, IntechOpen, 2023.

[12] J. Xiao, P. Liu, C. Wang, and G. Yang, “External field-assisted laser ablation in liquid: An efficient strategy for nanocrystal synthesis and nanostructure assembly,” *Prog. Mater. Sci.*, vol. 87, pp. 140–220, 2017.

[13] S. S. Abdullah, S. A. Salman, A. Kadhim, and A. M. Haleem, “Size control of Ag nanoparticles synthesized by PLA method in different liquid environments and their potent against virulent Candida Albicans,” *J Pharm Negat Results*, vol. 13, no. 4, pp. 423–431, 2022.

[14] N. Fadhil and F. Jasim, “Study of optical and structural properties of prepared gold nanoparticles by pulse laser ablation method,” *J. Educ. Sci.*, vol. 30, no. 4, pp. 60–69, 2021.

[15] Z. Najmudin, K. Krushelnick, E. L. Clark, D. J. Colling, M. Tatarakis, A. Modena, *et al.*, “The production of high-energy electrons from the interaction of an intense laser pulse with an underdense plasma,” *J. Mod. Opt.*, vol. 50, no. 3–4, pp. 673–681, 2003.

[16] R. A. Ismail, F. A. Fadhil, and H. H. Rashed, “Novel route to prepare lanthanum oxide nanoparticles for optoelectronic devices,” *Int. J. Mod. Phys. B*, vol. 34, no. 13, p. 2050134, 2020.

[17] A. M. Haleem, M. M. Taha, and A. A. Ayoub, “Anti-tumor and anti-oxidant effects of Ganoderma

lucidumextracts on oral squamous cell carcinoma and skin squamous cell carcinoma in vitro," *Curr. Issues Pharm. Med. Sci.*, vol. 37, no. 2, pp. 79–84, 2024.

[18] J. Jana, M. Ganguly, and T. Pal, "Enlightening surface plasmon resonance effect of metal nanoparticles for practical spectroscopic application," *RSC Adv.*, vol. 6, no. 89, pp. 86174–86211, 2016.

[19] D. Sevenler, N. L. Ünlü, and M. S. Ünlü, "Nanoparticle biosensing with interferometric reflectance imaging," *Nanobiosensors and Nanobioanalyses*, pp. 81–95, 2015.

[20] A. C. Pereira, A. E. F. Oliveira, M. A. C. Resende, and L. F. Ferreira, "Investigation of the Gold Nanoparticles Synthesis, Mechanism and Characterization Using the Turkevich Method," *Nanotechnology*, vol. 1, p. 3, 2023.

[21] G. Yogesh, S. Shukla, D. Sastikumar, and P. Koinkar, "Progress in pulsed laser ablation in liquid (PLAL) technique for the synthesis of carbon nanomaterials: a review," *Appl. Phys. A*, vol. 127, pp. 1–40, 2021.

[22] F. A. Fadhil, B. A. Hasoon, N. N. Hussein, and K. S. Khashan, "Preparation and characterization of CuO NPs via laser ablation under electric field and study their antibacterial activity," in *AIP Conference Proceedings*, AIP Publishing, 2018.

[23] Y. Ma, X. Wang, Z. Dong, X. Hou, T. Wang, W. Sun, *et al.*, "Effect of particle size on the microstructure and consolidation behavior of nickel coating fabricated by laser shockwave sintering," *J. Mater. Res. Technol.*, vol. 24, pp. 5404–5419, 2023.

[24] M. Wuithschick, A. Birnbaum, S. Witte, M. Sztucki, U. Vainio, N. Pinna, *et al.*, "Turkevich in new robes: key questions answered for the most common gold nanoparticle synthesis," *ACS Nano*, vol. 9, no. 7, pp. 7052–7071, 2015.

[25] U. Holzwarth and N. Gibson, "The Scherrer equation versus the'Debye-Scherrer equation'," *Nat. Nanotechnol.*, vol. 6, no. 9, p. 534, 2011.

[26] A. Kumar and A. S. Verma, "Lattice constant of orthorhomic perovskite solids," *J. Alloys Compd.*, vol. 480, no. 2, pp. 650–657, 2009.

[27] A. K. Ali, R. A. Khamis, and R. B. Rashid, "Preparation of Au-Ag composite Nanoparticles by Pulsed Laser Ablation in Water for controlling of AIP enzyme Activity in human blood," *J. Coll. basic Educ.*, vol. 25, no. 103, pp. 23–36, 2019.

[28] J. A. Saimon, R. O. Mahdi, A. A. Hadi, K. S. Khashan, F. A. Fadhil, I. H. Hadi, *et al.*, "Synthesis and characterization of Al_2O_3 nanoparticles using PLAL with different Nd: YAG laser fluences for photodetectors," *Plasmonics*, pp. 1–11, 2024.

[29] A. R. Ziefuß, S. Reichenberger, C. Rehbock, I. Chakraborty, M. Gharib, W. J. Parak, *et al.*, "Laser fragmentation of colloidal gold nanoparticles with high-intensity nanosecond pulses is driven by a single-step fragmentation mechanism with a defined educt particle-size threshold," *J. Phys. Chem. C*, vol. 122, no. 38, pp. 22125–22136, 2018.

[30] S. R. Park, H. W. Lee, J. W. Hong, H. J. Lee, J. Y. Kim, B. Choi, *et al.*, "Enhancement of the killing effect of low-temperature plasma on Streptococcus mutans by combined treatment with gold nanoparticles," *J. Nanobiotechnology*, vol. 12, pp. 1–8, 2014.

[31] K. Daliri, N. Seifi-Shalamzari, M. Saeida-Ardekani, S. Ekraminasab, and H. Neamatzadeh, "Application of Golden Nanoparticles against Streptococcus Mutans for Prevention of Caries Lesions," *World J. Peri Neonatol.*, 2020.

[32] A. Manke, L. Wang, and Y. Rojanasakul, "Mechanisms of nanoparticle-induced oxidative stress and toxicity," *Biomed Res. Int.*, vol. 2013, no. 1, p. 942916, 2013.

[33] M. Milić, G. Leitinger, I. Pavičić, M. Zebić Avdičević, S. Dobrović, W. Goessler, *et al.*, "Cellular uptake and toxicity effects of silver nanoparticles in mammalian kidney cells," *J. Appl. Toxicol.*, vol. 35, no. 6, pp. 581–592, 2015.

[34] L. Zhang, Y. Ma, Z. Wei, and L. Wang, "Toxicity of gold nanoparticles complicated by the co-existence multiscale plastics," *Front. Microbiol.*, vol. 15, p. 1447046, 2024.

[35] A. M. Haleem, A. H. Hameed, R. A. Al-Majeed, N. N. Hussein, R. A. Hikmat, and B. K. Queen, "Anticancer, antioxidant, antimicrobial and cytogenetic effects of ethanol leaves extract of Carthamus tinctorius," in *IOP Conference Series: Earth and Environmental Science*, IOP Publishing, 2023, p. 52035.

[36] H. H. Rashed, F. A. Fadhil, and I. H. Hadi, "Preparation and characterization of lead oxide nanoparticles by laser ablation as antibacterial agent," *Baghdad Sci. J.*, vol. 14, no. 4, p. 801, 2017.